



The prefrontal cortex of the bottlenose dolphin (*Tursiops truncatus* Montagu, 1821): a tractography study and comparison with the human

Tommaso Gerussi¹ · Jean-Marie Graïc¹ · Antonella Peruffo¹ · Mehdi Behroozi² · Lara Schlaffke³ · Stefan Huggerberger⁴ · Onur Güntürkün^{2,5} · Bruno Cozzi¹

Received: 10 May 2023 / Accepted: 21 August 2023 / Published online: 3 September 2023
© The Author(s) 2023

Abstract

Cetaceans are well known for their remarkable cognitive abilities including self-recognition, sound imitation and decision making. In other mammals, the prefrontal cortex (PFC) takes a key role in such cognitive feats. In cetaceans, however, a PFC could up to now not be discerned based on its usual topography. Classical *in vivo* methods like tract tracing are legally not possible to perform in Cetacea, leaving diffusion-weighted imaging (DWI) as the most viable alternative. This is the first investigation focussed on the identification of the cetacean PFC homologue. In our study, we applied the constrained spherical deconvolution (CSD) algorithm on 3 T DWI scans of three formalin-fixed brains of bottlenose dolphins (*Tursiops truncatus*) and compared the obtained results to human brains, using the same methodology. We first identified fibres related to the medio-dorsal thalamic nuclei (MD) and then seeded the obtained putative PFC in the dolphin as well as the known PFC in humans. Our results outlined the dolphin PFC in areas not previously studied, in the cranio-lateral, ectolateral and opercular gyri, and furthermore demonstrated a similar connectivity pattern between the human and dolphin PFC. The antero-lateral rotation of the PFC, like in other areas, might be the result of the telescoping process which occurred in these animals during evolution.

Keywords Cetacean · Brain evolution · Dolphin · PFC · CSD · DWI

Abbreviations

En	Entolateral sulcus	Ss	Suprasylvian sulcus
Es	Ectolateral sulcus	AC	Anterior commissure
La	Lateral sulcus	CC	Corpus callosum
Sf	Sylvian fissure	Cl	Cingulate cortex
		CSD	Constrained spherical deconvolution
		DTI	Diffusion tensor imaging
		DWI	Diffusion-weighted imaging
		ES	Ectolateral gyrus
		MC	Motor cortex
		MDN	Medio-dorsal thalamic nucleus
		MGN	Medial geniculate nucleus
		LG	Lateral gyrus
		LGN	Lateral geniculate nucleus
		OT	Optic tract
		PFC	Prefrontal cortex
		SS	Suprasylvian gyrus
		SSC	Somatosensory cortex

✉ Tommaso Gerussi
tommaso.gerussi@phd.unipd.it

¹ Department of Comparative Biomedicine and Food Science (BCA), University of Padua, Legnaro, Italy

² Department of Biopsychology, Institute of Cognitive Neuroscience, Faculty of Psychology, Ruhr-University Bochum, 44801 Bochum, Germany

³ Department of Neurology, BG-University Hospital Bergmannsheil, Ruhr-University Bochum, Bürkle-de-La-Camp-Platz 1, 44789 Bochum, Germany

⁴ Institute of Anatomy and Clinical Morphology, Witten/Herdecke University, Alfred-Herrhausen-Straße 50, 58448 Witten, Germany

⁵ Research Center One Health Ruhr, Research Alliance Ruhr, Ruhr-University Bochum, Bochum, Germany

Introduction

The bottlenose dolphin *Tursiops truncatus* (Montagu, 1821) is a member of the *Delphinidae* family often kept in captivity, and consequently frequently studied. Individuals of this species may perform a large variety of complex cognitive tasks including sound imitation, understanding of human syntax, conceptual decision taking, understanding numerosity, and self-recognition (Kilian et al. 2003; Kuczaj et al. 2009; Herman 2012; Yaman et al. 2012; Güntürkün 2014; Loth et al. 2022). Bottlenose dolphins demonstrated a capacity for complex planning and to devise composite hunting strategies (Tyack 2009; Herman 2012; Loth et al. 2022). In terrestrial mammals, these executive functions, elaborate behavioural actions, and the required working memory, are regulated by the prefrontal cortex (PFC; Fuster 2015), a neocortical area deemed responsible for higher brain functions in humans (Tranel et al. 2003; Butler and Hodos 2005; Kandel et al. 2021). The PFC is the “cortex of the anterior pole of the brain” and defined as the major receiver of thalamic inputs from the medio-dorsal nucleus (MDN) (Petrides and Pandya 2012; Fuster 2015). The MDN indeed projects also to the cingulate, insular premotor and parietal cortices (May and Forutan 2012). The identification of the PFC, as for other areas, is, therefore, based on composite anatomical landmarks and functional experiments that result in well-accepted cortical maps of the human brain compared to the dolphin brain (Fig. 1a, b). The topographical concept of PFC has been applied to the brain of lab rodents, domestic carnivores, sheep, rabbit, and primates, and validated functionally mostly through invasive studies (Rose and Woolsey 1948; Dinopoulos et al. 1985; Fuster 2015).

The brain of the bottlenose dolphin weighs approx. 1600 g and has roughly 3700 cm² of cortical surface, which are higher absolute values compared to the human brain (1300 g and 2400 cm², respectively; Ridgway and

Brondson 1984; Hofman 1985; Cozzi et al. 2017). The current neocortical maps for this species (See Chapter 6 in Cozzi et al. 2017; Chapter 5 in Huguenberger et al. 2019) derive almost entirely from early direct, intracortical evoked potential studies (Lende and Akdikmen 1968; Ladygina and Supin 1970, 1974; Lende and Welker 1972; Sokolov et al. 1972; for review, see Bullock and Gurevich 1979; Supin et al. 2001; Cozzi et al. 2017) and retrograde tracing (Garey and Revishchin 1990). These pioneering studies allowed the tentative identification and preliminary topography of key functional areas, including motor (MC), somatosensory (SSC), primary and secondary auditory (A1, A2), and primary and secondary visual (V1, V2) cortices (Fig. 1b, c). No further invasive studies were published afterwards, due to growing ethical concerns and public awareness of animal rights. A large part of the dolphin cerebral cortex remains, therefore, unexplored, and several functions are still not mapped topographically.

The absence of an experimentally based topographical identification of the associative areas of the bottlenose dolphins (and other cetacean species) represents a potential critical point that limits neuroanatomical comparisons and potentially hampers even behavioural studies (for discussion, see Chapter 10 in Cozzi et al. 2017). To date, the PFC has not been delineated in dolphins, and the topography of the rostral portion of the cortex in dolphins does not clearly match that of terrestrial mammals, including artiodactyls. What has been stated so far is that the antero-ventral (“frontal” or “orbital”) part of the dolphin brain contains very large pyramidal cells, attributable to a putative motor cortex (see Kojima 1951; Hof et al. 2005). However, the variety and complexity of behaviours briefly described above suggest the existence of an area at least partially functionally homologous to the human PFC. To further support this hypothesis, here we emphasise that the thalamic nuclei (including the MDN) that in primates and rodents are usually related to associative cortical targets, are markedly developed in the

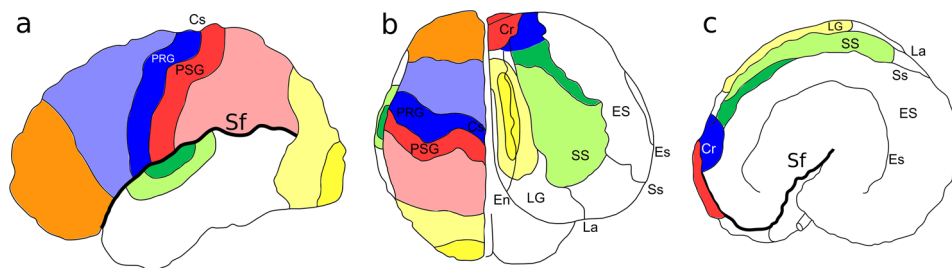


Fig. 1 Neocortical brain map of **a** human in left view, **b** human (left hemisphere) and dolphin (right hemisphere) in dorsal view and **c** dolphin in left view. Dark blue, Motor cortex; light blue, premotor cortex; Red, somatosensory cortex; light red, associative somatosensory cortex; yellow, V1; light yellow, associative visual cortex; dark green, A1; light green, associative auditory cortex; orange, PFC. Cr cruciate

ate sulcus, *Cs* central sulcus, *En* entolateral sulcus, *ES* ectosylvian gyrus, *Es* ectosylvian sulcus, *La* lateral sulcus, *LG* lateral gyrus, *PRG* precentral gyrus, *PSG* postcentral gyrus, *Sf* Sylvian fissure, *SS* suprasylvian gyrus, *Ss* suprasylvian sulcus. Neocortical maps adapted from Martin (2021; human) and Cozzi et al. (2017, dolphin)

Table 1 Origin of specimens

Species	ID	Sex	Age	Origin	Cause of death	Fixation interval	Imaging interval
<i>T. truncatus</i>	# 4	F	Adult	Marine theme park	Drowning	< 12 h	21 yr
	# 9	F		Marine theme park	Septicaemia	< 12 h	20 yr
	# 457	M		Wild	NA	< 12 h	2 yr
<i>H. sapiens</i>	MGH 1007	M	Adult	Not applicable	NA	NA	NA
	MGH 1010	F					
	MGH 1016	M					
	MGH 1019	F					
	MGH 1031	M					

The age class was known in the captive animals and estimated in the wild due to its total length (Jefferson et al. 2015)

dolphin (Kruger 1959, 1966). A recent publication on the brains of the spotted and common dolphins (Berns et al. 2015) described a thalamo-temporal pathway, based on the use of Diffusion Tensor Imaging (DTI). The striatal projections from the basal ganglia to the “frontal” lobes were investigated as well and a similar connectivity pattern to primates was found. Nevertheless, these findings were presented as a validation of the technique compared to the other data analysed and no further assumption about a putative PFC in cetaceans was present (Berns et al. 2015).

Invasive tracing studies in live dolphins are now ethically unacceptable, and similar considerations may prevent MR studies of healthy dolphins anaesthetised only for research purposes. Furthermore, many research and clinical MRI bores and coils may be unfit for the large head of the species. Consequently, DTI and other diffusion-weighted imaging (DWI) techniques on whole-fixed brains represent one of the few ethical and practical approaches to study connectivity patterns, but their applications to dolphins have been rare.

DTI was the first mathematical algorithmic method to encode DWI in a 3D tensor model with 6 degrees of freedom and perform tractography. Since the tensor model only represents the most dominant diffusion orientation, crossing fibres are not considered (Basser 1995). To overcome this known problem, a new algorithm, the Constrained Spherical Deconvolution (CSD), was developed. CSD is based on the acquisition of High Angular Resolution Diffusion Imaging (HARDI) and its model includes the possibility of multiple dominant diffusion orientations as in crossing fibres and, therefore, allows a better understanding of the organisation of fibre tracts (Tournier et al. 2007; Calamuneri et al. 2018).

CSD and other DWI methods are mathematical models that provide an interpretation of biological barriers within the brain. These methods are susceptible to artefacts, and the resulting data must be carefully interpreted. Tractography algorithms cannot distinguish between inputs and outputs, or rather, do not add a sense to the direction of the fibres, and as such, the words “terminated” (or similar) should be interpreted bearing in mind this caveat. Despite this limitation,

DWI methods are currently the only non-invasive techniques available for studying structural brain connectivity (Schilling et al. 2020).

In the present study, we investigated whether the bottlenose dolphins possess an area with the topographical and connection characteristics of the human PFC, as detected by CSD. To this effect, we acquired post-mortem DW images on three adult bottlenose dolphin brains and performed tractography using CSD to investigate the fibre pathways involving the MDN. The results were compared with parallel investigations on the human brain.

Materials and methods

Origin of the specimens

Information on the bottlenose dolphin ($n = 3$) and human ($n = 5$) brains used in the present study are reported in Table 1.

Dolphin brains were extracted during routine necropsy performed at the Department of Comparative Biomedicine and Food Science (BCA) of the University of Padova (Italy) on specimens stranded on the Veneto coast. The brains were consequently fixed in phosphate buffered paraformaldehyde (4%) and stored in the *Mediterranean marine mammal tissue bank* (MMMTB, <http://www.marinemammals.eu>), located in BCA. The MMMTB is a CITES recognised (IT020) research centre, sponsored by and collaborating with the Italian Ministry of the Environment and the University of Padova. MMMTB collects and stores samples from wild or captive marine mammals whose samples or whole carcasses are delivered to BCA for post-mortem diagnostics.

Alive human brains were obtained from the Human Connectome Project (HCP) database (<https://ida.loni.usc.edu/login.jsp>). HCP is supported by the National Institute of Dental and Craniofacial Research (NIDCR), the National Institute of Mental Health (NIMH) and the National Institute of Neurological Disorders and Stroke (NINDS). The HCP is

the result of efforts of co-investigators from the University of Southern California, Martinos Center for Biomedical Imaging at Massachusetts General Hospital (MGH), Washington University, and the University of Minnesota.

ID 9 was cut in the mid-sagittal plane for other research purposes. Anyway, both hemispheres were scanned together. In this case, any fibre going to the contralateral hemisphere was considering false.

Data acquisition

Dolphins

Brain scans were acquired using a 3 T MRI human whole body system (Achieva 3 T X, Philips) and a 32-channel head coil. A 3D fast acquisition with Fast Field Echo Imaging (FFE) was used to obtain high-resolution T2-weighted structural images. The parameters were: TFE factor = 105; field of view (FOV) = $150.0 \times 200.0 \times 150.0$ mm³; repetition time/echo time (TR/TE) = 8.2/3.8 ms; matrix size (MTX) = 152×201 ; 150 slices with a voxel size of $1.0 \times 1.0 \times 1.0$ mm³. Acquisition time per brain was 6.26 min. DW images were obtained using an Echo Planar Imaging (EPI) series with following parameters: EPI factor of 41; FOV = $224 \times 168 \times 150$ mm³; TR/TE = 23,200/88 ms; MTX = 112×82 ; 75 slices with a voxel size of $2.0 \times 2.0 \times 2.0$ mm³. 60 gradient directions with $b = 3500$ s/mm² and 1 non-diffusion-weighted image ($b = 0$ s/mm²) were acquired. Acquisition time per brain was 24 min and 21 s. An additional DW image with 2 gradient direction ($b = 3500$ s/mm²) and 2 non-diffusion-weighted images were acquired in the opposite phase encoding direction for the subsequent motion/distortion correction. The protocol used at the beginning was specific for DWI image acquisition in live humans. Accordingly, various sequences were tested at the beginning by changing the b values and resolution to obtain the best SNR under those conditions. Considering all the three dolphins, the SNR, calculated as the mean signal of each gradient in the raw data, ranged for the $b = 0$ s/mm² from 36.6 to 40 and for the $b = 3500$ s/mm² from 13 to 16.

Humans

Human scans were acquired using a customised Siemens 3 T Connectom scanner, which is a modified 3 T Skyra system (MAGNETOM Skyra Siemens Healthcare) with 64-channel tight-fitting brain array coil. A 3D MPRAGE sequence was used to obtain T1w structural images with the following parameters: FOV 256×256 mm; TR/TE 2530/1.15 ms; voxel size of $1.0 \times 1.0 \times 1.0$ mm³. Acquisition time per brain was 6.02 min. Additional T2w structural images were acquired with 3D T2-SPACE sequence with the following parameters: FOV 224×224 mm; TR/TE

3200/561 ms; voxel size of $0.7 \times 0.7 \times 0.7$ mm³. Acquisition time per brain was 6.48 min. DW images were obtained using a Spin-echo EPI sequence with: FOV = 210×210 mm; TR/TE = 8800/57 ms; MTX = 140×140 ; 96 slices with a voxel size of $1.5 \times 1.5 \times 1.5$ mm³. 64 gradient directions with $b = 1000$ s/mm², 64 gradient directions with $b = 3000$ s/mm², 128 gradient directions with $b = 5000$ s/mm² and 2 sets of 128 gradient directions with $b = 10,000$ s/mm² were acquired. Every 14 volumes, a $b = 0$ image was collected, and 1 non-diffusion-weighted image ($b = 0$ s/mm²) was acquired. Acquisition time per brain was 89 min.

More information on the human brain scans can be found at the following link: <https://www.humanconnectome.org/study/hcp-young-adult/document/mgh-adult-diffusion-data-acquisition-details/>.

Data processing

Dolphins

Data were processed through FSL (<https://fsl.fmrib.ox.ac.uk/fsl/fslwiki>; Smith et al. 2004; Woolrich et al. 2009; Jenkinson et al. 2012) and MRtrix3 (<https://www.mrtrix.org/>; Tournier et al. 2012) toolboxes. Briefly, images were denoised (Veraart et al. 2015, 2016), corrected from Gibb's ringing artefacts (Kellner et al. 2015), corrected for EPI-distortion (Holland et al. 2010), b_0 -field inhomogeneity (Andersson et al. 2003; Smith et al. 2004), Eddy-current and movement (Andersson and Sotiropoulos 2016). Subsequently, the dhollander algorithm was applied to compute different response functions for the white matter (WM, anisotropic), cerebrospinal fluid and grey matter (CSF and GM, both isotropic). Finally, the fibre orientation distribution (FOD) was calculated before the elaboration of the tractography (Dhollander et al. 2016a, b, 2017; Tournier et al. 2019). Each brain was then investigated individually.

Humans

Preprocessed data of human brains were already present in the HCP files, but further steps were added in order to create a template atlas, averaging all five subjects. Images were corrected from bias field and group DWI intensity normalisation was performed. In these data, there were 4 shells, therefore, the dhollander algorithm was used to estimate different response functions and then average them to calculate the FOD. Once all subjects' FOD were complete, we created a population template, a template mask and warping all the FOD images to the template space (for reference, see Tournier et al. 2019).

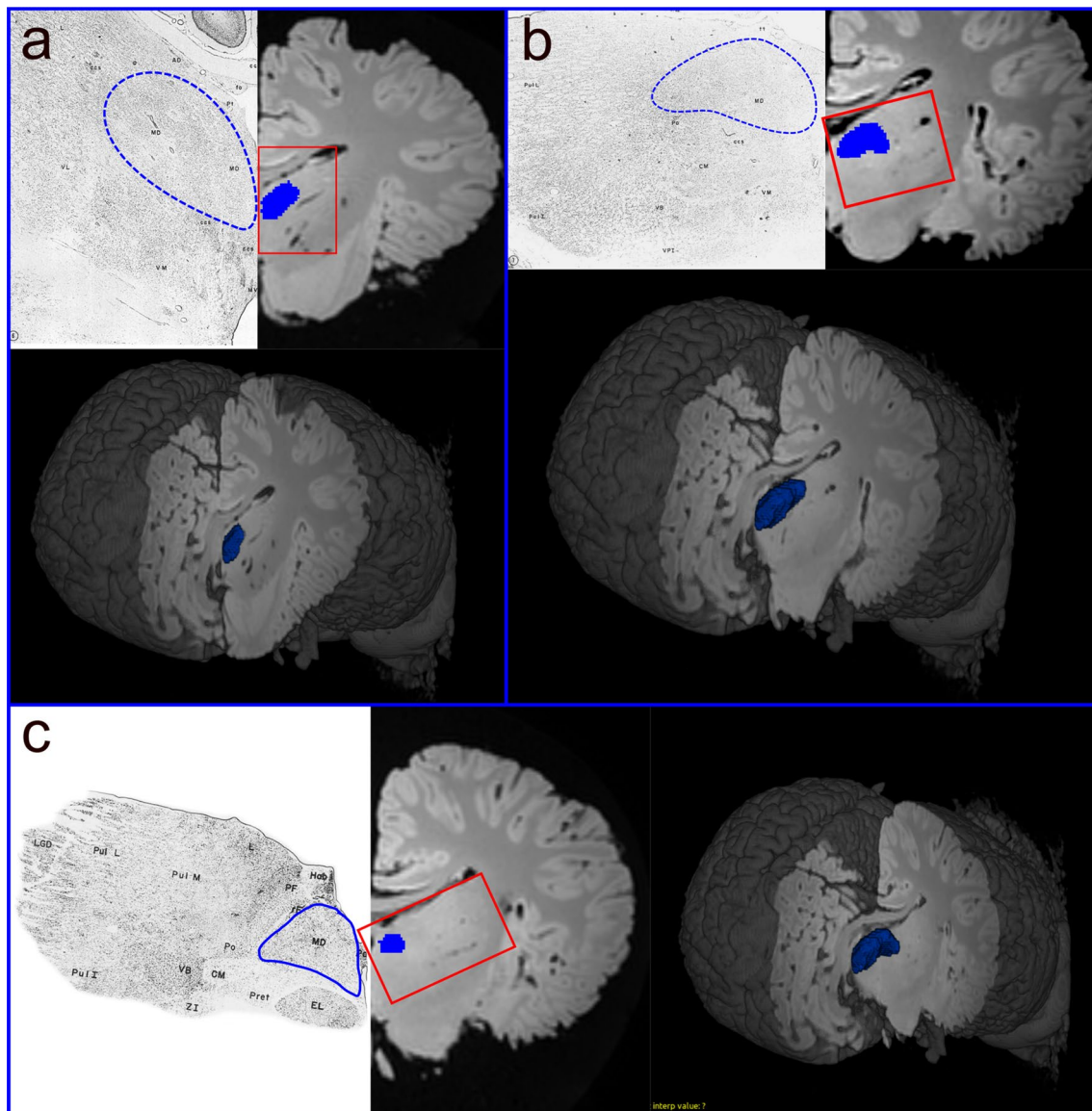


Fig. 2 Representation of the MDN mask based on the panels described by Kruger (1959) and Morgane and Jacobs (1972). The directions from **a** to **c** are rostro-caudal with a 3D visualisation of

the section and the whole mask at the correspondent plane; **a** section taken based on panel number 6; **b** section taken based on panel number 7; **c** section taken based on panel number 3

Tractography

Throughout the following, the procedure was applied to both right and left hemispheres. In dolphins, the MDN mask was manually drawn using the ITK-SNAP software (Yushkevich et al. 2016; www.itk-snap.org; version 3.8.0) following the topographical location described by Kruger (1959) and Morgane and Jacobs (1972). The thalamic subdivision is quite evident in the histological data if compared to our MRI data. We first identified the thalamic topographic position based on the histology, and then drew the areas. Since the slides did not include all the thickness of the thalamus, we tried to reconstruct the missing space following its shape (Fig. 2).

The final mask was intentionally slightly eroded to avoid the generation of erroneous extra fibres. Since there is no map of the PFC location in *Cetacea*, a PFC area was first created, based from the tracts originating from the MDN. To verify that the tracts were not artefactual, we restricted the tracking using the designated PFC as the seed image and reaching the MDN nucleus, thus restraining the fibres to the bundle only connecting one with the other.

In the human, MDN and PFC were manually drawn with ITK-SNAP, based on the currently available templates and atlases (Tamraz and Comair 2000; Cho 2010; Ding et al. 2016). For both dolphin and human brains, fibre tracking was performed through a deterministic algorithm based on

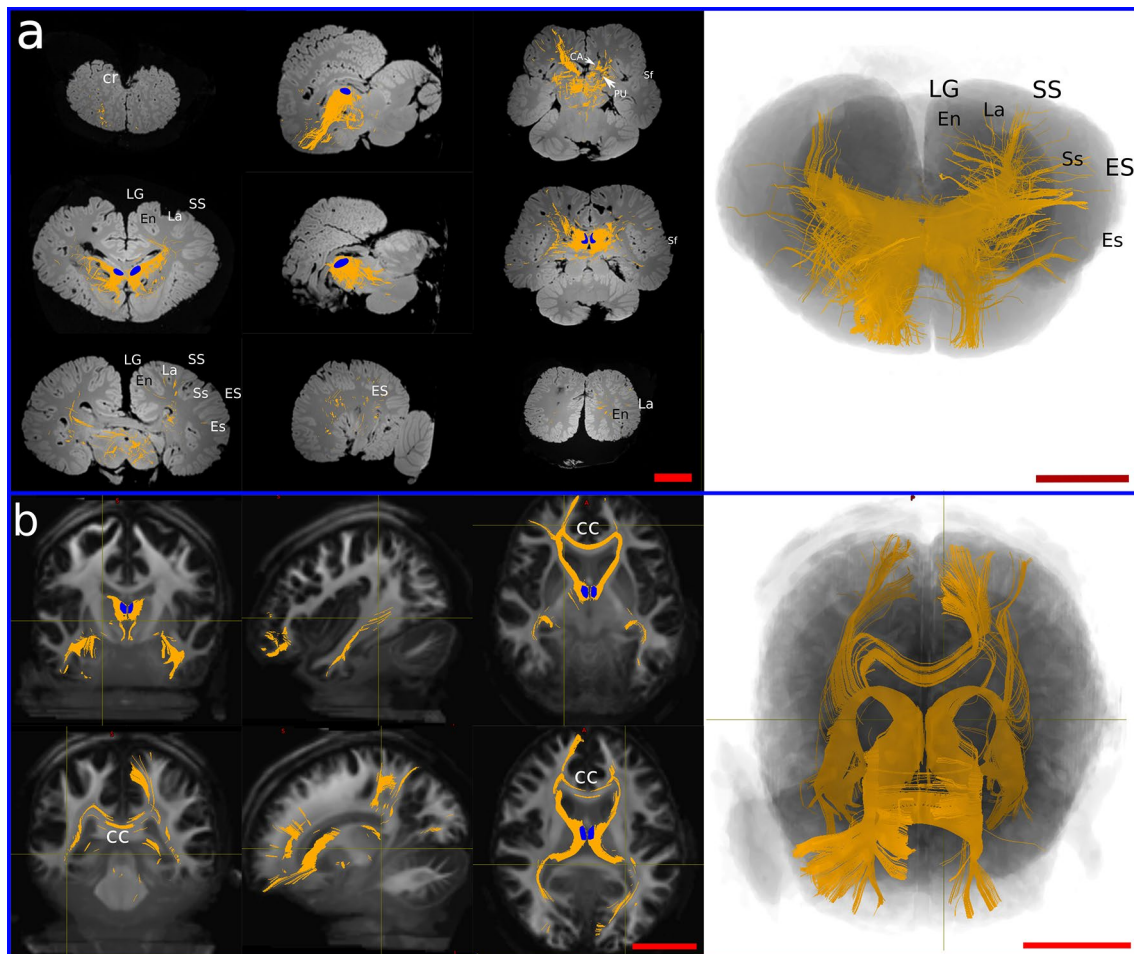


Fig. 3 Prefrontal pathways in the dolphin and human brains. **a** Tracts generated from seeding the MDN (blue shape) in dolphin. **b** Tracts generated from seeding MDN (blue shape) in human. *CC* corpus

callosum, *En* entolateral sulcus, *Es* ectolateral sulcus, *ES* ectolateral gyrus, *La* lateral sulcus, *LG* lateral gyrus, *Sf* sylvian fissure, *Ss* suprasylvian sulcus, *SS* suprasylvian gyrus. Red scale bar = 5 cm

CSD, with the FOD file as input and the following parameters: FA threshold 0.1 for dolphin brains (as they were fixed) and 0.2 for human brains (since the subjects were alive), step size 0.1 mm, default angle threshold 60°, and default streamline count (5000).

Results

Seeding point: MDN nuclei

In the dolphin brains, the main fibre bundles exiting the MDN were directed cranially running below the cruciate sulcus (Cr) towards the ventro-cranial pole, passing between the Putamen (PU) and caudate nucleus (CA). Other consistent fibre bundles went dorsally following the internal capsule and terminated in i) the supralimbic cortex around the entolateral sulcus (En), the lateral sulcus (La), and the suprasylvian sulcus (Ss); then ii) laterally

in the temporal lobes around the ectolateral sulcus (Es). Some tracts ran caudally to the Edinger–Westphal nucleus (EW), the Interstitial Nucleus of Cajal (INC) and the elliptic nucleus (NE), then moved ventrally towards the crus cerebri (Fig. 2a). Projections from the MDN were also commonly distributed within the thalamus and then ran to other brain areas. Few aberrant fibres passed through the superior colliculi (SC) (Fig. 3a).

In the human brain, fibres ran to the PFC following the anterior thalamic peduncle, then went laterally to the temporal lobe following the inferior thalamic peduncle. Some of the latter fibres split from the inferior thalamic bundle to join the optic radiation directed towards the parietal lobe. We also noted fibres that reached the CC to spread in the contralateral hemisphere (Fig. 3b).

Thanks to our previous results, we were able to estimate a presumptive frontal region based on the extension of the fibres on the WM tracts (Fig. 4).

Fig. 4 Putative PFC (red mask) based on previous projections from the MD (blue mask). **a** Frontal view; **b** dorsal view

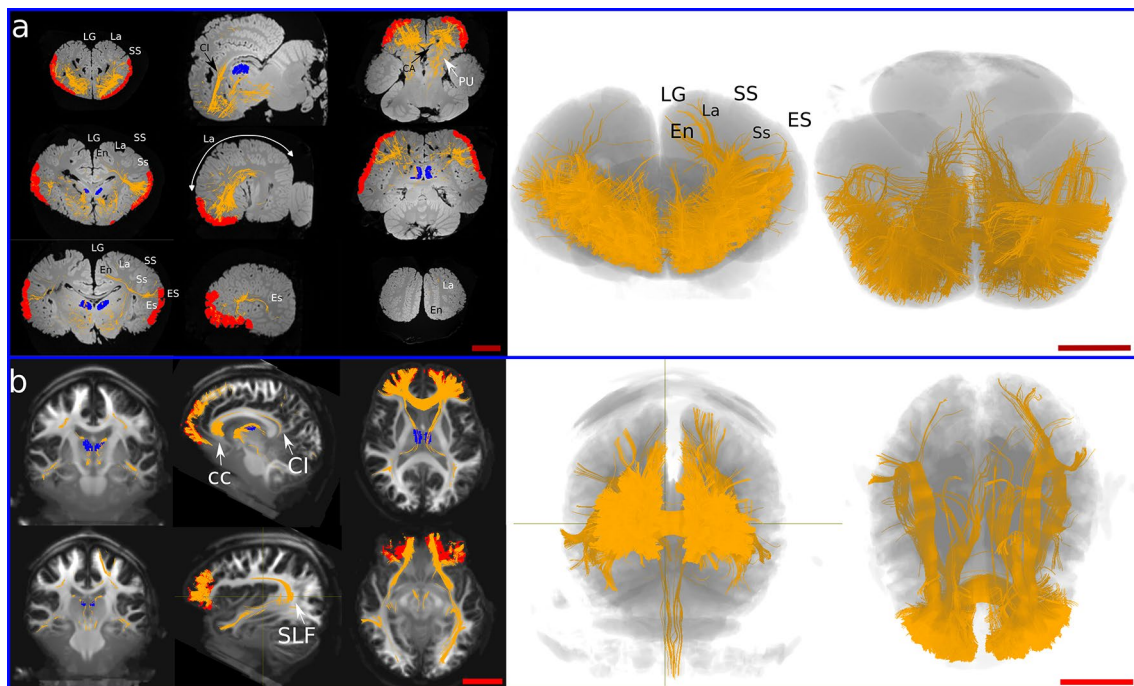
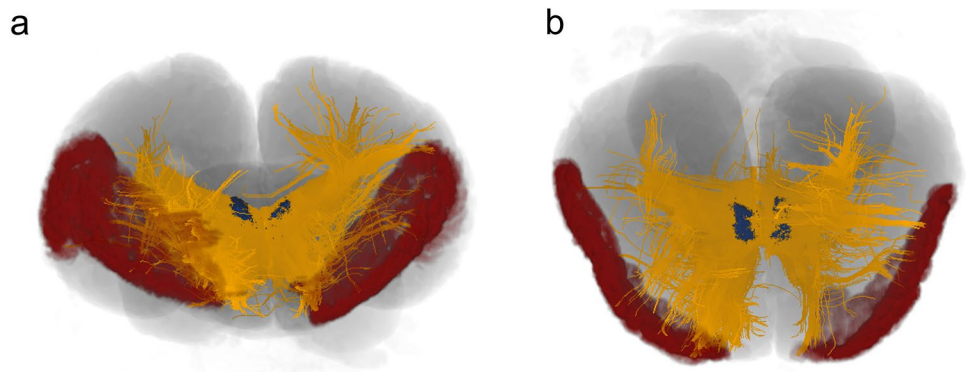


Fig. 5 Prefrontal pathways in the dolphin and human brains. **a** Tracts generated from seeding the PFC (red shape) in dolphin. **b** Tracts generated from seeding PFC (red shape) in human. The MDN is represented in blue. *CA* caudate nucleus, *CC* corpus callosum, *CI* cingu-

lum, *En* entolateral sulcus, *Es* ectolateral sulcus, *ES* ectolateral gyrus, *La* lateral sulcus, *LG* lateral gyrus, *PU* putamen, *SLF* superior longitudinal fasciculus, *Ss* suprasylvian sulcus, *SS* suprasylvian gyrus. Red scale bar=5 cm

Seeding point: acquired PFC

Seeding the putative PFC resulted in the presence of several ipsilateral U-shaped fibres within the area. Other fibre tracts were oriented towards the basal ganglia and the cingulate cortex (CI). Other bundles continued through the MDN to end in the pons. A consistent number of fibres joined the superior longitudinal fasciculus (SLF) directed to the temporal lobe (Es, Ss) while others arose to En and La (Fig. 5a). Finally, some tracts reached the CC and crossed contralaterally.

In the human brain, ipsilateral fibres created from the PFC joined the inferior fronto-occipital fasciculus and reached the VI. Other fibres joined the fornix, then ran caudally towards the MDN, the CI. Some tracts were directed to the temporal lobe apparently through the SLF. Fibres directed towards the mesencephalon reached the periaqueductal grey and the red nucleus in the tegmentum (Fig. 5b). Finally, consistent fibre bundles moved to the CC and then crossed to the contralateral hemisphere.

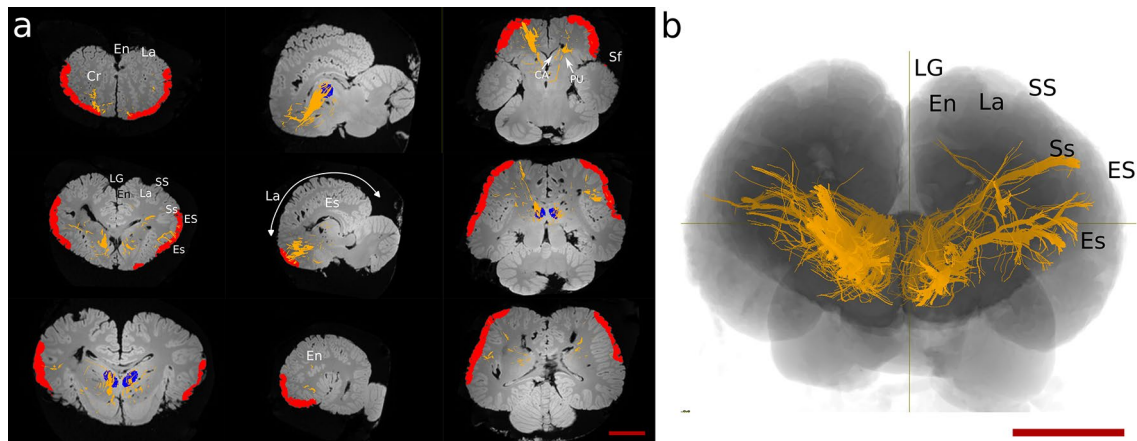
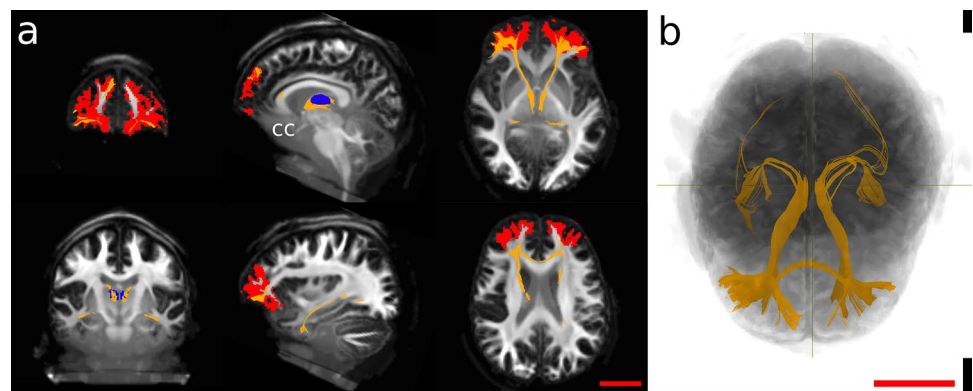


Fig. 6 Constrained tractography between the putative found PFC (red shape) and the MDN (blue shape). *CA* caudate nucleus, *Cr* cruciate sulcus, *En* entolateral sulcus, *Es* ectolateral sulcus, *ES* ectolateral

gyrus, *La* lateral sulcus, *LG* lateral gyrus, *PU* putamen, *Sf* sylvian fissure, *Ss* suprasylvian sulcus, *SS* suprasylvian gyrus

Fig. 7 Constrained tractography between the putative found PFC (red shape) and the MDN (blue shape). *CC* corpus callosum



Specifically constrained thalamo-cortical connections

To delimit the fibres previously generated singularly from the MDN nuclei or from the presumptive PFC, we also selectively constrained the tracking between these two regions.

In general, these fibres were fewer and more limited. In the dolphin, cortically seeded bundles passed below the *Cr* and between the basal ganglia to reach the MDN. Other streamlines ran laterally to the temporal lobe (*Ss*, *Es*), and very few fibres continued dorsally to the ENs and LAs. Finally, some fibre bundles were directed caudally to the red nucleus and the elliptic nucleus (Fig. 6).

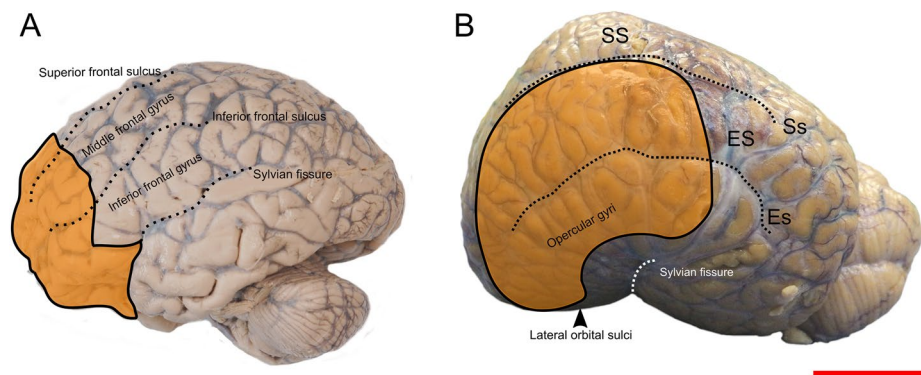
Prefrontal pathways in the human brain between PFC and MDN also crossed through the *CC* and reached the temporal lobe of the contralateral hemisphere through the inferior thalamic peduncle. Few fibres detached from the inferior thalamic peduncle and continued caudally until the *VC* (Fig. 7).

Discussion

A precise identification of the topography and connectivity of the PFC (or its homologue) in dolphins represents a consistent step forward towards the understanding of their brain architecture and the neural basis for some of the complex behaviours of the species. To the best of our knowledge, DWI technique is currently one of the very few technically feasible and ethically acceptable approaches to identify the PFC in dolphins, and potentially other large ex-vivo brains.

In the present study, we performed CSD-based tractography and aimed at identifying fibre tracts that connect selected thalamic nucleus to their related cortical targets/origin. We then compared the data with those obtained in the human brain. Since the human PFC is one of the key areas assigned to higher brain functions (Tranel et al. 2003; Butler and Hodos 2005; Kandel et al. 2021), we searched for an area in the dolphin brain with the same characteristic connections.

Fig. 8 Approximate PFC representation (orange area) in human (A) and dolphin (B) brain. For abbreviations, see the list. Red scale bar = 5 cm



CSD is a HARDI algorithm of DWI that, within the limits of human clinical MRI parameters, can reconstruct crossing fibres within a voxel, thus giving a more plausible biological result (Arrigo et al. 2016; Jeurissen et al. 2017). The algorithm can be applied and extended also to fixed brains, much like with DTI (D’Arceuil and de Crespigny 2007; Rane and Duong 2011; Gerussi et al. 2022). Classical retrograde and anterograde tract-tracing remains the gold standard methodology to accurately study brain connections. However, the technique was seldom performed in cetacean brains, and likely will not be in the future because of the ethical constraints briefly outlined in the Introduction. In this context, opportunistic fixed-brain DWI (and its various algorithmic variations), therefore, constitutes an adequate method to investigate brain connections in these mammals, even considering its biases and limits to interpretation (Jeurissen et al. 2017; Schilling et al. 2020). Fixation produces microstructural changes such as dehydration or tissue degeneration, which in turn may alter some MRI parameters including SNR, FA and apparent diffusion coefficient (ADC) (D’Arceuil and de Crespigny 2007; Rane and Duong 2011). Therefore, the obtained results must consider all the limitations of DWI in general and DWI applied to fixed tissues.

Tracing and tractography in dolphins and porpoises

Literature on evoked potential placed the bottlenose dolphin V1/V2 around En in the LG, extending rostro-caudally and with the La as its lateral boundary. A1/A2 develops from there along the SS, reaching the Ss with a rostro-caudal direction (for review see Supin et al. 2001). According to the literature, the Cr separates rostrally the medial SSC from the lateral MC. Other reports that used tracing in the harbour porpoise (*Phocoena phocoena*) established the existence of projections from the parvocellular part of the MGN to the suprasylvian and ectosylvian gyri (Krashnoshchekova and Figurina 1980; Voronov et al. 1985), and the involvement of the LGN as target of the optic nerve. Evoked potentials were used also for track-tracing-based injections in various areas of the neocortex (LG, the SS, ES, temporal and orbital) of

the harbour porpoise (Revishchin and Garey 1990). Overall, the data obtained showed that medial thalamic projections progressively crossed to a lateral cortical position, therefore, ending contralaterally to their origin (see Revishchin and Garey 1990, Fig. 13). However, no tracing study was ever performed on a putative PFC.

A recent DTI study described for the first time the existence of a direct auditory pathway from IC to MGN to the temporal lobe near the Sylvian fissure in the common (*Delphinus delphis*) and pantropical spotted dolphin (*Stenella attenuata*), and an overlap of thalamic visual and auditory pathways (Berns et al. 2015). Such direct pathways, often hypothesised, but never demonstrated before, suggest a direct and profound interconnection of the dolphin visual and auditory system. Nevertheless, given the extremely limited data concerning the functional auditory region in cetaceans, it should be considered a still partially unsolved scientific question.

Topography and characterisation of the PFC in the human and dolphin brain

The human PFC can be divided into four functional areas: orbitofrontal cortex (OFC), dorsolateral PFC (dlPFC), dorsomedial PFC (dmPFC) and ventromedial PFC (vmPFC) (Kolb 2015). The caudolateral boundaries of the PFC roughly correspond to the cranial part of the precentral sulcus (premotor cortex) and medially to the cingulate cortex. The Brodmann areas overlapping the human PFC are: BA8–14, 24, 25, 32, 44–47 (Murray et al. 2017). These are marked by notable cytoarchitectural differences that determine their boundaries (Brodmann’s 2006; Petrides and Pandya 2012). Although the frontal lobe possess its own cytoarchitectural peculiarity (Hof et al. 2005), there are no such characteristic differences in the bottlenose dolphin, and other cetaceans in general (Kern et al. 2011; van Kann et al. 2017). We started by identifying topographical landmarks that may characterise comparatively the dolphin PFC (see orange area in the Fig. 8) and then proceeded with CSD tractography. The average mass of the brain in the bottlenose dolphin is

1.550 g (Huggenberger et al. 2019), vs. the average value of 1300–1400 g for the human (Miller and Corsellis 1977) must be taken in account. Without discussing the body and brain weight correlation, or the Encephalization Quotient¹ (Jerison 1973; for discussion of its application to cetaceans see Cozzi et al. 2016), we emphasise that the position of the area occupied by the PFC, based on topographically equivalent landmarks, appears more lateral in the dolphin brain comparatively to man, even considering the different brain shape and dimensions.

Prefrontal pathways

In the human DWI scans, seeding the human MDN (Fig. 2b) resulted in fibres that reached most of the PFC through the anterior thalamic peduncle, while some other fibres joined the inferior thalamic peduncle and were then oriented towards the somatosensory association area in the parietal lobe and V1. Our results were consistent with those found by Grodd et al. (2020). When the same method was applied to the brains of the bottlenose dolphins, the resulting fibres joined the internal capsule, passed between the basal ganglia towards the ventro-cranial pole and ended ventrally to the Cr. Other fibres were directed towards either the LGN or the MGN, going through the internal capsule and terminating in the parietal lobe. We also noted that some fibres were directed caudally, possibly to merge in post-thalamic tectal pathways. A putative PFC could be identified in the bottlenose brain by mapping fibres that reached the non-parietal neocortex (Fig. 8). The projections arising from this putative PFC then continued (a) within the PFC itself; (b) moved to the contralateral PFC through the CC; (c) to the CI; (d) to the pons passing between the basal ganglia and MDN; or (e) to the temporal lobe following the SLF. The connectivity pattern detected in the bottlenose brain was in fact similar to that found in the human brain.

To check whether these fibres were not just artefactual, we first seeded the MDN to establish where the fibres were going. Then we seeded the designated area to see if some of the fibres projected independently back to the MDN. We noticed that some fibres again connected the PFC with the MDN, but other bundles were oriented towards different areas. The PFC is a multimodal association area which receives and sends inputs to other brain regions, and—to this effect—our results were consistent with what reported in the literature (Fuster 2015). We finally constrained the seeding between the two areas to qualitatively see the amount of fibres only related to these seeds, and exclude other

unspecific bundles. We found a more marked asymmetry in the dolphin brains compared to human brains (Figs. 6 and 7), but given the scope of our study and its qualitative approach, we did not emphasise this aspect.

The acquisition parameters used to scan the live human brains (referred to the HCP) were evidently better than those of the (dead) dolphin brains. However, we detected no substantial loss of signal in the formalin-fixed dolphin brains, so that identification of a putative PFC area in their brain gave results that were largely comparable to the human. No former tracking or injection studies based on evoked potential reported a functional identification of a putative PFC in dolphin, hence, this is the first report of a putative PFC in this species, and, to the best of our knowledge, in all cetaceans. Its boundaries start in the orbital lobe, extend laterally in the cranial ES and reach the cranial opercular lobe. However, additional fibres were connected to areas placed below the SSC and MC cortices, in which pyramidal neurons were previously found (Manger 2006).

According to the concept of the “initial brain” (for reference see Glezer et al. 1988, Fig. 7) modern mammals still retain some key topographical features already present in the brains of their early ancestors, notwithstanding the divergent evolutionary path of the taxa. The enlarged human neocortex contains far more and varied cortical modules than in primordial mammals. The cetacean brain obviously followed a different evolutionary route since the brain mantle greatly expanded to the uttermost known limits for mammals in terms of relative cortical size, while the cytoarchitecture is poorly differentiated and mostly homogeneous in the neocortex (Cozzi et al. 2017).

In the human brain, the development of the PFC displaced all the areas caudally, thus modifying the primeval topographical scheme (Fig. 9). In cetaceans, the progressive evolution to life in the water caused a wide range of body structure modifications. In the head specifically, the growth of the melon, the telescoping process, and the nasal shift which caused the change of the cranial axes and shape, might have prevailed over the longitudinal development of the brain (Miller 1923; Cozzi et al. 2017; Roston and Roth 2019). Consequently, the brain folded around the insula (see dotted arrows in Fig. 9) and expanded more laterally: what in terrestrial mammals is “caudal” becomes “dorsal” in the dolphin and so forth (Morgane and Jacobs 1972). Concomitant space limits within the cerebral cavity prompted a striking cortical gyrification and induced the topographical shift of neocortical areas. Our data based on CSD tractography confirmed that the (evolutionary) process that modified the cetacean brain was compatible with the persistence of a very large and richly connected PFC area.

The PFC of terrestrial mammals, and the correspondent areas in birds, are highly innervated by dopaminergic neurons (Sawaguchi and Goldman-Rakic 1991; Gaspar et al.

¹ EQ [EQ = $E^i / 0.12 \times P^{2/3}$; E^i = mean brain weight, P = mean body weight] is 3.79 in the bottlenose dolphin vs. 6.62 in man, according to Huggenberger et al. (2019)

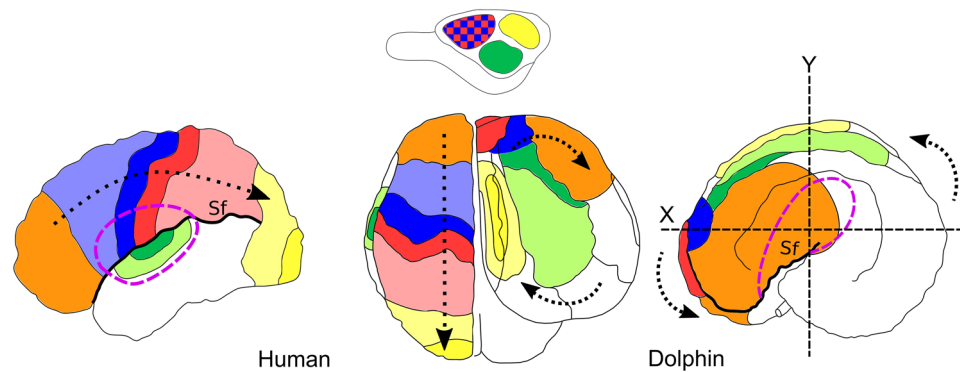


Fig. 9 Schematic picture of the brain evolution from its “initial” form (top, Glezer et al. 1988) to the dolphin (Jacobs et al. 1984; Cozzi et al. 2017) and human (Martin 2021) brains (bottom). Orange, PFC; Blue, SSC; Red, MC; Green, A1/A2; Yellow, V1/V2. Sf, Sylvian fissure. Dashed purple line delimits the border of the insular cortex.

The dotted arrow in the human brain indicates the displacement of the other areas due to the expansion of the PFC. The dotted arrows in the dolphin brain indicate the rotation of the organ around the insular cortex and the probable cranio-lateral shift of the PFC and other cortical areas on the surface. X, Y body axes

1992; Güntürkün 2005). Based on this neurochemical concept, further studies are needed to investigate the actual presence of dopaminergic neurons in the PFC of dolphins. This is particularly important in the fronto-ventral area, where one should not expect to find an associative cortex (Manger 2006, referring to Kojima 1951), and in the lateral (opercular) area. Additional functional MRI (fMRI) or recently developed functional near-infrared spectroscopy (fNIRS) techniques (Scholkmann et al. 2014) might also become useful for the study of brain functions through the proxy of increased blood flow during local stimulation, very similar to blood-oxygen-level-dependent contrast in fMRI. A composite multidisciplinary approach may eventually shed light on the unmapped cortical fields of these mammals with remarkable cognitive abilities.

Acknowledgements The authors thank the Human Connectom Project for the available data used in this manuscript. (Principal Investigators: Bruce Rosen, M.D., Ph.D., Arthur W. Toga, Ph.D., Van J. Weeden, M.D.). HCP funding was provided by the National Institute of Dental and Craniofacial Research (NIDCR), the National Institute of Mental Health (NIMH) and the National Institute of Neurological Disorders and Stroke (NINDS). HCP data are disseminated by the Laboratory of Neuro Imaging at the University of Southern California).

Author contributions Conceptualisation: TG, OG, BC; methodology: TG, MB, LS; formal analysis and investigation: TG, JMG, AP, SH, BC; writing—original draft preparation: TG; writing—review and editing: JMG, MB, LS, SH, OG, BC; funding acquisition: OG, BC; supervision: JMG, MB, LS, SH, OG, BC.

Funding Open access funding provided by Università degli Studi di Padova within the CRUI-CARE Agreement. This work was supported by a grant from the German Research Council to OG (Gu 227/16-1), and from the University of Padova D.O.R. Bruno Cozzi.

Data availability The datasets generated during and/or analysed during the current study are available from the corresponding author on reasonable request.

Declarations

Conflict of interest The authors declare no competing interests.

Ethical approval The dolphin brains used in this study were sampled during routine necropsies at the University. Therefore, no animals were deliberately killed for the purpose of this study. The human scans were freely accessible on the Human Connectom Project website, under the condition of adding them in the acknowledgments.

Consent to participate Not applicable.

Consent to publish Not applicable.

Open Access This article is licensed under a Creative Commons Attribution 4.0 International License, which permits use, sharing, adaptation, distribution and reproduction in any medium or format, as long as you give appropriate credit to the original author(s) and the source, provide a link to the Creative Commons licence, and indicate if changes were made. The images or other third party material in this article are included in the article’s Creative Commons licence, unless indicated otherwise in a credit line to the material. If material is not included in the article’s Creative Commons licence and your intended use is not permitted by statutory regulation or exceeds the permitted use, you will need to obtain permission directly from the copyright holder. To view a copy of this licence, visit <http://creativecommons.org/licenses/by/4.0/>.

References

- Andersson JLR, Sotiropoulos SN (2016) An integrated approach to correction for off-resonance effects and subject movement in diffusion MR imaging. *Neuroimage* 125:1063–1078. <https://doi.org/10.1016/j.neuroimage.2015.10.019>

- Andersson JLR, Skare S, Ashburner J (2003) How to correct susceptibility distortions in spin-echo echo-planar images: application to diffusion tensor imaging. *Neuroimage* 20:870–888. [https://doi.org/10.1016/S1053-8119\(03\)00336-7](https://doi.org/10.1016/S1053-8119(03)00336-7)
- Arrigo A, Calamuneri A, Mormina E (2016) Diffusion MRI: from principles to modelling and clinical applications. Biomedical imaging. Dover, SmGroup, pp 1–18
- Basser PJ (1995) Inferring microstructural features and the physiological state of tissues from diffusion-weighted images. *NMR Biomed* 8:333–344. <https://doi.org/10.1002/nbm.1940080707>
- Berns GS, Cook PF, Foxley S, Jbabdi S, Miller KL, Marino L (2015) Diffusion tensor imaging of dolphin brains reveals direct auditory pathway to temporal lobe. *Proc R Soc B* 282:20151203. <https://doi.org/10.1098/rspb.2015.1203>
- Brodman K (2006) Localisation in the cerebral cortex. Springer, New York. <https://doi.org/10.1007/b138298>
- Bullock TH, Gurevich VS (1979) Soviet literature on the nervous system and psychobiology of cetacea. *Int Rev Neurobiol*. [https://doi.org/10.1016/s0074-7742\(08\)60637-6](https://doi.org/10.1016/s0074-7742(08)60637-6)
- Butler AB, Hodos W (2005) Comparative vertebrate neuroanatomy: evolution and adaptation. John Wiley & Sons, Hoboken
- Calamuneri A, Arrigo A, Mormina E et al (2018) White matter tissue quantification at low b-values within constrained spherical deconvolution framework. *Front Neurol*. <https://doi.org/10.3389/fneur.2018.00716>
- Cho Z-H (2010) 7.0 Tesla MRI brain atlas. Springer, New York. <https://doi.org/10.1007/978-1-60761-154-7>
- Cozzi B, Mazzariol S, Podestà M et al (2016) An unparalleled sexual dimorphism of sperm whale encephalization. *Int J Comp Psychol*. <https://doi.org/10.46867/ijcp.2016.29.00.01>
- Cozzi B, Huggenberger S, Oelschläger H (2017) Brain, spinal cord, and cranial nerves. In: Cozzi B, Huggenberger S, Oelschläger H (eds) Anatomy of dolphins. Elsevier, Amsterdam, pp 197–304. <https://doi.org/10.1016/b978-0-12-407229-9.00006-3>
- D’Arceuil H, de Crespigny A (2007) The effects of brain tissue decomposition on diffusion tensor imaging and tractography. *Neuroimage* 36:64–68. <https://doi.org/10.1016/j.neuroimage.2007.02.039>
- Dhollander T, Connelly A (2016a) Generating a T1-like contrast using 3-tissue constrained spherical deconvolution results from single-shell (or multi-shell) diffusion MR data. *Conf ISMRM Work Break Barriers Diffus. MRI*
- Dhollander T, Raffelt D, Connelly A (2016b) Unsupervised 3-tissue response function estimation from single-shell or multi-shell diffusion MR data without a co-registered T1 image. In: *Confence: ISMRM Works Break Barriers Diffus. MRI*. Lisbon, Portugal, p 5
- Dhollander T, Raffelt D, Connelly A (2017) Towards interpretation of 3-tissue constrained spherical deconvolution results in pathology. *Proc Intl Soc Mag Reson Med* 25:1815
- Ding S, Royall JJ, Sunkin SM et al (2016) Comprehensive cellular-resolution atlas of the adult human brain. *J Comp Neurol* 524:3127–3481. <https://doi.org/10.1002/cne.24080>
- Dinopoulos A, Karamanlidis AN, Papadopoulos G et al (1985) Thalamic projections to motor, prefrontal, and somatosensory cortex in the sheep studied by means of the horseradish peroxidase retrograde transport method. *J Comp Neurol* 241:63–81. <https://doi.org/10.1002/cne.902410106>
- Fuster JM (2015) Anatomy of the prefrontal cortex. *Prefrontal Cortex*. <https://doi.org/10.1016/b978-0-12-407815-4.00002-7>
- Garey LJ, Revishchin AV (1990) Structure and thalamocortical relations of the cetacean sensory cortex: histological, tracer and immunocytochemical studies. In: Thomas JA, Kastelein RA (eds) Sensory abilities of cetaceans. Springer, New York, pp 19–30. https://doi.org/10.1007/978-1-4899-0858-2_2
- Gaspar P, Stepniewska I, Kaas JH (1992) Topography and collateralization of the dopaminergic projections to motor and lateral prefrontal cortex in owl monkeys. *J Comp Neurol* 325:1–21. <https://doi.org/10.1002/cne.903250102>
- Gerussi T, Graic J-M, Grandis A et al (2022) The orbitofrontal cortex of the sheep. Topography, organization, neurochemistry, digital tensor imaging and comparison with the chimpanzee and human. *Brain Struct Funct* 227:1871–1891. <https://doi.org/10.1007/s00429-022-02479-w>
- Glezer II, Jacobs MS, Morgane PJ (1988) Implications of the “initial brain” concept for brain evolution in Cetacea. *Behav Brain Sci* 11:75–89. <https://doi.org/10.1017/s0140525x0005281x>
- Grodd W, Kumar VJ, Schüz A et al (2020) The anterior and medial thalamic nuclei and the human limbic system: tracing the structural connectivity using diffusion-weighted imaging. *Sci Rep*. <https://doi.org/10.1038/s41598-020-67770-4>
- Güntürkün O (2005) The avian ‘prefrontal cortex’ and cognition. *Curr Opin Neurobiol* 15:686–693. <https://doi.org/10.1016/j.conb.2005.10.003>
- Güntürkün O (2014) Is dolphin cognition special? *Brain Behav Evol* 83:177–180. <https://doi.org/10.1159/000357551>
- Herman LM (2012) Body and self in dolphins. *Conscious Cogn* 21(1):526–545. <https://doi.org/10.1016/j.concog.2011.10.005>
- Hof PR, Chanis R, Marino L (2005) Cortical complexity in cetacean brains. *Anat Rec* 287A:1142–1152. <https://doi.org/10.1002/ar.a.20258>
- Hofman MA (1985) Size and shape of the cerebral cortex in mammals. *Brain Behav Evol* 27:28–40. <https://doi.org/10.1159/000118718>
- Holland D, Kuperman JM, Dale AM (2010) Efficient correction of inhomogeneous static magnetic field-induced distortion in echo planar imaging. *Neuroimage* 50:175–183. <https://doi.org/10.1016/j.neuroimage.2009.11.044>
- Huggenberger S, Oelschläger H, Cozzi B (2019) The nervous system. In: Huggenberger S, Oelschläger H, Cozzi B (eds) Atlas of the anatomy of dolphins and whales. Elsevier, Amsterdam, pp 323–362. <https://doi.org/10.1016/b978-0-12-802446-1.00005-9>
- Jacobs MS, Galaburda AM, McFarland WL, Morgane PJ (1984) The insular formations of the dolphin brain: quantitative cytoarchitectonic studies of the insular component of the limbic lobe. *J Comp Neurol* 225:396–432
- Jefferson TA, Webber MA, Pitman RL (2015) Cetaceans. In: Jefferson TA, Webber MA, Pitman RL (eds) Marine mammals of the world. Elsevier, Amsterdam, pp 24–357. <https://doi.org/10.1016/b978-0-12-409542-7.50004-4>
- Jenkinson M, Beckmann CF, Behrens TEJ et al (2012) FSL *Neuroimage* 62:782–790. <https://doi.org/10.1016/j.neuroimage.2011.09.015>
- Jerison HJ (1973) Evolution of the brain and intelligence. Academic Press, New York
- Jeurissen B, Descoteaux M, Mori S, Leemans A (2017) Diffusion MRI fiber tractography of the brain. *NMR Biomed*. <https://doi.org/10.1002/nbm.3785>
- Kandel ER, Koester JD, Mack SH, Siegelbaum SA (2021) Principles of neural science, 6th edn. McGraw-hill, New York
- Kellner E, Dhital B, Kiselev VG, Reiser M (2015) Gibbs-ringing artifact removal based on local subvoxel-shifts. *Magn Reson Med* 76:1574–1581. <https://doi.org/10.1002/mrm.26054>
- Kern A, Siebert U, Cozzi B et al (2011) Stereology of the neocortex in odontocetes: quantitative, and functional implications. *Brain Behav Evol* 77:79–90. <https://doi.org/10.1159/000323674>
- Kilian A, Yaman S, von Fersen L, Güntürkün O (2003) A bottlenose dolphin discriminates visual stimuli differing in numerosity. *Anim Learn Behav* 31:133–142. <https://doi.org/10.3758/bf03195976>
- Kojima T (1951) On the brain of the sperm whale (Physeter catodon L.). *Sci Rep Whales Res Inst Tokyo* 6:49–72
- Kolb B (2015) Prefrontal cortex. *Int Encycl Soc Behav Sci*. <https://doi.org/10.1016/b978-0-08-097086-8.55045-4>

- Krasnoshchekova EI, Figurina II (1980) Korkovye proektsii medial'nogo kolenchatogo tela mozga del'fina. *Arkh Anat Gistol Embriol* 4:19–24
- Kruger L (1959) The thalamus of the dolphin (*Tursiops truncatus*) and comparison with other mammals. *J Comp Neurol* 111:133–194. <https://doi.org/10.1002/cne.901110107>
- Kruger L (1966) Specialized features of the cetacean brain. In: Norris KS (ed) Whales, dolphins and porpoises. University of California Press, University, pp 232–254
- Kuczaj II SA, Gory JD, Xitco MJ Jr (2009) How intelligent are dolphins? A partial answer based on their ability to plan their behavior when confronted with novel problems. *Jpn J Anim Psychol* 59:99–115. <https://doi.org/10.2502/janip.59.1.9>
- Ladygina TF, Supin AI (1970) Acoustic projection in the dolphin cerebral cortex. *Fiziologicheskii Zhurnal SSSR Imeni IM Sechenova* 56(11):1554–1560
- Ladygina TF, Supin AY (1974) Morphology, physiology and acoustics of marine mammals. Nauka, Moscow
- Lende RA, Akdikmen S (1968) Motor field in cerebral cortex of the bottlenose dolphin. *J Neurosurg* 29:495–499. <https://doi.org/10.3171/jns.1968.29.5.0495>
- Lende RA, Welker WI (1972) An unusual sensory area in the cerebral neocortex of the bottlenose dolphin, *Tursiops truncatus*. *Brain Res* 45:555–560. [https://doi.org/10.1016/0006-8993\(72\)90482-9](https://doi.org/10.1016/0006-8993(72)90482-9)
- Loth A, Güntürkün O, von Fersen L, Janik VM (2022) Through the looking glass: how do marked dolphins use mirrors and what does it mean? *Anim Cogn* 25:1151–1160. <https://doi.org/10.1007/s10071-022-01680-y>
- Mai JK, Forutan F (2012) Thalamus. In: Mai JK, Paxinos G (eds) The human nervous system. Elsevier, Amsterdam, pp 618–677. <https://doi.org/10.1016/B978-0-12-374236-0.10019-7>
- Manger PR (2006) An examination of cetacean brain structure with a novel hypothesis correlating thermogenesis to the evolution of a big brain. *Biol Rev* 81:293. <https://doi.org/10.1017/s1464793106007019>
- Martin JH (2021) Neuroanatomy, 5th edn. McGraw-hill, New York
- Miller GS (1923) The telescoping of the cetacean skull (with eight plates). *Smithson Misc Collect* 76:1
- Miller AKH, Corsellis JAN (1977) Evidence for a secular increase in human brain weight during the past century. *Ann Hum Biol* 4:253–257. <https://doi.org/10.1080/03014467700007142>
- Morgane PJ, Jacobs MS (1972) Comparative anatomy of the cetacean nervous system. In: Harrison RJ (ed) Functional anatomy of marine mammals, vol 1. Academic Press, Cambridge, pp 117–244
- Murray EA, Wise SP, Graham KS (2017) The evolution of memory systems: ancestors, anatomy, and adaptations. Oxford University Press, Oxford
- Petrides M, Pandya DN (2012) The frontal cortex. In: Mai JK, Paxinos G (eds) The human nervous system. Elsevier, Amsterdam, pp 988–1011. <https://doi.org/10.1016/b978-0-12-374236-0.10026-4>
- Rane S, Duong TQ (2011) Comparison of in vivo and ex vivo diffusion tensor imaging in rhesus macaques at short and long diffusion times. *Open Neuroimag J* 5:172–178. <https://doi.org/10.2174/1874440001105010172>
- Revishchin AV, Garey LJ (1990) The thalamic projection to the sensory neocortex of the porpoise, *Phocoena phocoena*. *J Anat* 169:85–102
- Ridgway SH, Brownson RH (1984) Relative brain sizes and cortical surface areas in odontocetes. *Acta Zool Fenn* 172:149–152
- Rose JE, Woolsey CN (1948) Structure and relations of limbic cortex and anterior thalamic nuclei in rabbit and cat. *J Comp Neurol* 89(3):279–347. <https://doi.org/10.1002/cne.900890307>
- Roston RA, Roth VL (2019) Cetacean skull telescoping brings evolution of cranial sutures into focus. *Anat Rec* 302:1055–1073. <https://doi.org/10.1002/ar.24079>
- Sawaguchi T, Goldman-Rakic PS (1991) D1 dopamine receptors in prefrontal cortex: involvement in working memory. *Science* 251:947–950. <https://doi.org/10.1126/science.1825731>
- Schilling KG, Petit L, Rheault F et al (2020) Brain connections derived from diffusion MRI tractography can be highly anatomically accurate—if we know where white matter pathways start, where they end, and where they do not go. *Brain Struct Funct* 225:2387–2402. <https://doi.org/10.1007/s00429-020-02129-z>
- Scholkmann F, Kleiser S, Metz AJ et al (2014) A review on continuous wave functional near-infrared spectroscopy and imaging instrumentation and methodology. *Neuroimage* 85:6–27. <https://doi.org/10.1016/j.neuroimage.2013.05.004>
- Smith SM, Jenkinson M, Woolrich MW et al (2004) Advances in functional and structural MR image analysis and implementation as FSL. *Neuroimage* 23:S208–S219. <https://doi.org/10.1016/j.neuroimage.2004.07.051>
- Sokolov VE, Ladygina TF, Supin AI (1972) Localization of sensory zones in the dolphin cerebral cortex. *Doklady Akademii Nauk SSSR* 202(2):490–493. <http://www.ncbi.nlm.nih.gov/pubmed/4333815>
- Supin AY, Popov VV, Mass AM (2001) The Sensory Physiology of Aquatic Mammals. Springer, US. <https://doi.org/10.1007/978-1-4615-1647-7>
- Tamraz JC, Comair YG (2000) Atlas of regional anatomy of the brain using MRI. Springer-Verlag. <https://doi.org/10.1007/3-540-30672-2>
- Tournier J-D, Calamante F, Connelly A (2007) Robust determination of the fibre orientation distribution in diffusion MRI: non-negativity constrained super-resolved spherical deconvolution. *Neuroimage* 35:1459–1472. <https://doi.org/10.1016/j.neuroimage.2007.02.016>
- Tournier J-D, Calamante F, Connelly A (2012) MRtrix: diffusion tractography in crossing fiber regions. *Int J Imaging Syst Technol* 22:53–66. <https://doi.org/10.1002/ima.22005>
- Tournier J-D, Smith R, Raffelt D et al (2019) MRtrix3: a fast, flexible and open software framework for medical image processing and visualisation. *Neuroimage* 202:116137. <https://doi.org/10.1016/j.neuroimage.2019.116137>
- Tranel D, Cooper G, Rodnitzky RL (2003) Higher brain functions. In: Conn PM (ed) Neuroscience in medicine. Humana Press, New Jersey, pp 621–639. https://doi.org/10.1007/978-1-59259-371-2_29
- Tyack PL (2009) Behavior, overview. In: Perrin WF, Würsig B, Thewissen JGM (eds) Encyclopedia of marine mammals. Elsevier, Amsterdam, pp 101–108. <https://doi.org/10.1016/b978-0-12-373553-9.00029-8>
- van Kann E, Cozzi B, Hof PR, Oelschläger HHA (2017) Qualitative and quantitative analysis of primary neocortical areas in selected mammals. *Brain Behav Evol* 90:193–210. <https://doi.org/10.1159/000477431>
- Veraart J, Fieremans E, Novikov DS (2015) Diffusion MRI noise mapping using random matrix theory. *Magn Reson Med* 76:1582–1593. <https://doi.org/10.1002/mrm.26059>
- Veraart J, Novikov DS, Christiaens D et al (2016) Denoising of diffusion MRI using random matrix theory. *Neuroimage* 142:394–406. <https://doi.org/10.1016/j.neuroimage.2016.08.016>
- Voronov VA, Krasnoshchekova EI, Stosman IM, Figurina II (1985) Morphofunctional organization and cortical projections of the medial geniculate body in the harbour porpoise *Phocaena phocaena*. *J Evol Biochem Phys* 21(1):45–51
- Woolrich MW, Jbabdi S, Patenaude B et al (2009) Bayesian analysis of neuroimaging data in FSL. *Neuroimage* 45:S173–S186. <https://doi.org/10.1016/j.neuroimage.2008.10.055>
- Yaman S, Kilian A, von Fersen L, Güntürkün O (2012) Evidence for a numerosity category that is based on abstract qualities of “few” vs “many” in the bottlenose dolphin (*Tursiops truncatus*). *Front Psychol*. <https://doi.org/10.3389/fpsyg.2012.00473>

Yushkevich PA, Gao Y, Gerig G (2016) ITK-SNAP: An interactive tool for semi-automatic segmentation of multi-modality biomedical images. In 2016 38th annual international conference of the IEEE engineering in medicine and biology society (EMBC). IEEE. pp. 3342–3345

Publisher's Note Springer Nature remains neutral with regard to jurisdictional claims in published maps and institutional affiliations.